Optical properties and electronic structures of $B2$ and $B19'$ phases of equiatomic Ni-Ti alloys

Joo Yull Rhee
Department of Physics, College of Natural Sciences, Hoseo University, Asan, 336-795 Choongnam, Korea

B. N. Harmon and D. W. Lynch
Ames Laboratory-U.S. Department of Energy and Department of Physics and Astronomy, Iowa State University, Ames, Iowa 50011
(Received 13 July 1998)

The dielectric functions of equiatomic Ni-Ti alloys were measured by spectroscopic ellipsometry in the energy range of 1.5–5.4 eV at ~423 and at ~25 K. The peak at ~2.26 eV in the $B19'$ (monoclinic structure) optical conductivity spectrum has a slightly larger magnitude than in the $B2$ (cubic CsCl structure) phase, while the shoulder at ~3.5 eV becomes weaker and almost indiscernible upon martensitic transformation. A new structure develops at ~2.85 eV in the $B19'$ phase; however, it is also very weak. The band structures and the optical conductivity were calculated in both phases using the linearized-augmented-plane-wave method within the local-density approximation. **k** points near the Γ-X-M plane in the $B2$ phase and the corresponding **k**-points in $B19'$ phase contribute significantly to all three structures. The difference between the two spectra is due to the transitions between the folded-back bands from the $B2$ phase because of the larger unit cell of the $B19'$ phase and the change in the electronic energy spectrum near the Fermi level. The overall optical properties of Ni-Ti alloys in the measured energy range are rather insensitive to the martensitic transformation because the states far from the Fermi level are mainly involved in the interband transitions. [S0163-1829(99)06403-6]

I. INTRODUCTION

The intermetallic NiTi compound undergoes a martensitic transformation (MT) from the austenitic $B2$ phase at high temperature ($\geqslant$333 K) to the martensitic $B19'$ phase upon cooling.[1] The compound has been studied extensively because of its peculiar structural phase transition as well as its technological importance. It exhibits the so-called shape-memory effect[2] that accompanies the MT. If the alloy has a particular shape at a temperature above T_M ($\equiv$333 K) and is deformed into another shape at a temperature below T_M, it ''remembers'' and transforms back to its original shape upon heating above T_M. The transition also shows large hysteresis in electrical resistivity, Hall coefficient, sound velocity,[3] and magnetic susceptibility[3–5] upon cooling and heating.

After the first observation of the MT, Wang and his colleagues[2] explained the MT as an electronic phase transition such that at least some of the valence electrons become ''metallic'' (delocalized: NiTi-II) from ''covalent'' (localized: NiTi-III) at the MT.[3] This electronic charge transfer is described by shifting the *s*-band relative to the *d* band. The Fermi level increases about 1.1 eV, while the shapes of the *s*- and the *d*-band density of states (DOS) do not vary.[6] This model could successfully explain the low-temperature specific heat, magnetic susceptibility, enthalpy and Hall coefficient changes during the MT. However the Fermi energy shift is rather large. Furthermore soft-x-ray appearance potential spectroscopy measurements[7] show that there is no evidence of band structure shifts and give an upper limit of 0.1 eV on any change of the width of the empty *d*-band, which is an order of magnitude smaller than the 1.1 eV shift of the Fermi level estimated by Mitchell, Wang, and Cullen.[6] It was also shown that the electron transfer between Ni and Ti atoms accompanies changes in stoichiometry but is not characteristic of the $B2 \rightarrow B19'$ phase transition.

Shabalovskaya *et al.*[4] suggested that an electronic charge redistribution upon MT occurs, accompanied by the variation of the Fermi surface without any essential energy displacement. The idea of the variation of the Fermi surface was further developed by Egorushkin[8,9] by investigating the Fermi surface nesting and electron-phonon interaction. Zhao and co-workers[10,11] also investigated the phonon anomaly in β-phase NiTi. They used a first-principles linear-combination-of-atomic-orbitals method to calculate the energy band structure, which was fitted with a non-orthogonal tight-binding Hamiltonian. The nesting effects of the Fermi surface were found and phonon dispersion curves were calculated. The Fermi surface nesting causes the phonon mode near $Q_0=(\frac{2}{3},\frac{2}{3},0)(\pi/a)$, arising from strong electron-phonon coupling, to go soft. This is responsible for the pre-martensitic transition, the $B2 \rightarrow R$ (intermediate phase) transition.

Fermi surface nesting led to an alternative point of view.[12] A static distortion of the conduction-electron density and the lattice [charge-density wave (CDW)] occurs during a MT. The divergence is due to the geometrical peculiarities of the Fermi surface, so **q** is determined by the Fermi surface nesting.[12]

There are several band-structure calculations of $B2$ phase NiTi. The first self-consistent augmented-plane-wave calculation[13] showed Fermi surface nesting, which is closely related to anomalies of the phonon dispersion observed in inelastic neutron scattering[14] and ultrasonic attenuation experiments.[15] The authors also suggested that the nesting effects are related to an incommensurate CDW.[13]

Eibler, Redinger, and Neckel[16] calculated the band structures of intermetallic compounds MTi (M=Fe, Co and Ni)

in the $B2$ structure. The calculated x-ray photoemission spectra were in good agreement with experiment if a self-energy correction was employed. They recently calculated the band structures of NiTi and PdTi in the $B2$ phase.[17] The calculated DOS with lifetime broadening showed a close resemblance with measured photoelectron spectra. Their band structure is almost the same as that of Ref. 13 except for some differences in the symmetry assignment of the eigenvalues and one missing band. However, Lapin *et al.*[18] show somewhat different results from these two calculations, especially around the M point.

There are several band structure calculations[19–21] for NiTi in the $B19'$ phase. Recently Ye, Chan, and Ho[21] studied the structural and electronic properties of martensitic alloys (NiTi, PdTi, and PtTi). They used first-principles total-energy calculations to determine the equilibrium structure and concluded that the ground-state martensitic phase ($B19'$) is indeed lower in energy than the high-temperature $B2$ phase. The lowering of energy is associated with the lowering of the DOS at the Fermi level at the Ti site and the broadening of the Ni d band in the $B19'$ phase, indicating stronger bonding between Ni and Ti in the martensitic phase.

Recently Wang *et al.*[22] calculated the optical conductivity (OC) spectra of various transition-metal titanides in the $B2$ and $B19$ or $B19'$ phases. They used the equilibrium structural data obtained by the Ye *et al.*[21] and found a significant change in the OC spectra of NiTi alloys between the $B2$ and $B19'$ phases, especially in the 0.5–1.5 eV energy range where a substantial OC change was observed experimentally.[23] They also calculated the polarization dependent OC in the martensitic phase.

Nearly 20 years ago the dielectric functions for both phases were measured[23] by spectroscopic ellipsometry in the 0.07–4.9 eV range. Three peaks were observed in the $B2$ phase above 2 eV but only two peaks in the $B19'$ phase. However the magnitude does not change much upon MT. Some large changes occur below 1.5 eV. The structures below 1.5 eV are rich and change substantially upon MT, indicating an alteration of the electron energy spectrum in the vicinity of E_F. The authors claimed that the alteration is attributed to the opening of gaps in the $B19'$ phase, resulting from the splitting of degenerate d states.

The OC spectra were calculated earlier without inclusion of the dipole-transition matrix elements.[19,20] The calculated OC spectra for the $B2$ and $B19'$ phases agreed reasonably well with measured ones.[23] However, as shown below and elsewhere for Ni_3Al,[24] the inclusion of matrix elements, lifetime broadening, and the self-energy correction are very important for reliable comparison with experiment.

In this work we report the OC spectra measured in the energy range of 1.5–5.4 eV using a spectroscopic rotating-analyzer ellipsometer[25] and calculations of band structure and OC spectra for both phases. The dipole-transition matrix elements were taken into account for the OC calculations. The measured OC spectra did not show as many structures as those of Ref. 23 above 2 eV. Specifically we did not observe the peak around 2.6 eV. However, we observed a little change upon MT. For the $B19'$ phase calculation we used lattice parameters from new x-ray diffraction data[26] (slightly different from the previous measurement[1]), which give more reasonable band structures and DOS. The justification for using the new data is more thoroughly discussed by Ye, Chan, and Ho.[21]

II. EXPERIMENT

The alloy sample was produced by fusing iodine titanium and electrolytic nickel with purities of 99.999% in an electrolytic-arc furnace in a helium atmosphere. Sixfold fusion was used to ensure the homogeneity of the alloy sample. The weight loss was less than 0.1%. A nearly equiatomic NiTi alloy of composition $Ni_{49.8}Ti_{50.2}$ was finally prepared. It was then cut by a low-speed diamond saw to a shape appropriate for optical measurements. An optically reflecting surface was obtained by mechanical polishing with a series of alumina powders down to 0.05 μm diameter. The sample was then cleaned with acetone and methanol in an ultrasonic cleaner. We put the sample in an ultrahigh vacuum (UHV) chamber for high-temperature measurement. The high temperature ($\sim$423 K) was achieved by baking the whole chamber to 150 °C. During the baking we measured for the $B2$ phase. The $B19'$ phase was measured at $\sim$25 K, using a closed-cycle helium refrigerator. The spectroscopic rotating-analyzer ellipsometer and the closed-cycle helium refrigerator are described in detail elsewhere.[25] The $B19'$ phase is monoclinic, with three independent diagonal components in the OC tensor, and one off-diagonal component. Our polycrystalline sample was sufficiently fine grained that we measured an average of the components.

III. CALCULATIONS

The self-consistent band structures for both phases were calculated using a scalar-relativistic version of the linearized-augmented-plane-wave (LAPW) method[27] within the standard muffin-tin approximation for the potential. The spin-orbit interaction was included in the self-consistent iteration in such a way that the spin-orbit Hamiltonian was diagonalized after the scalar-relativistic bands and wave functions had been calculated. The core states were treated fully relativistically in the frozen core approximation. The muffin-tin radius was chosen so that each sphere almost touches the neighboring spheres. The potential was spherically symmetric inside the muffin tin and constant outside. Parameters used in the calculation are summarized in Table I. For the $B19'$ phase the inversion symmetry center was chosen as the origin. The local-density approximation of Hedin and Lundqvist[28] to the density-functional formalism was used to include the exchange-correlation contribution to the potential.

A 150–160 LAPW basis function set for the $B2$ phase and 235 to 255 LAPW basis function set for the $B19'$ phase, depending on the **k** point, were used for each self-consistent iteration. The energy eigenvalues at 120 **k** points in the irreducible Brillouin zone (IBZ $=\frac{1}{48}$ of the BZ) for the $B2$ phase were calculated. However, 250 **k** points in IBZ ($=\frac{1}{4}$ of the BZ) for the $B19'$ phase were used in the self-consistent iterations.

Once the self-consistent potential and charge were obtained, we calculated the DOS and OC spectra using the linear-energy-tetrahedron method.[29] The usual direct interband transitions were assumed for the OC calculation. 512

TABLE I. Parameters used in the calculations.

	$B2$	$B19'$
Latt. Const. (units=a.u.)	$a=5.6994$	$a=5.4764$ $b=8.7797$ $c=7.7630$ $\gamma=97.78°$
Atomic pos.	Ni(0,0,0)	Ni(0.0372,0.1752,0.25) Ni(−0.0372,−0.1752,−0.25)
	Ti(0.5,0.5,0.5)	Ti(0.4176,−0.2836,0.25) Ti(−0.4176,0.2836,−0.25)
Muffin-tin rad. (units=a.u.)	$R_{MT}^{Ni}=2.2549$ $R_{MT}^{Ti}=2.6362$	$R_{MT}^{Ni}=2.2549$ $R_{MT}^{Ti}=2.6362$
$R_{MT}K_{MAX}$	9.00	8.00

tetrahedra in the IBZ, corresponding to 24 576 tetrahedra in the whole BZ for the $B2$ phase, and 1536 tetrahedra in the IBZ corresponding to 6144 tetrahedra in the whole BZ for the $B19'$ phase were used in the calculation. For the $B19'$ phase the number of tetrahedra is $\frac{1}{4}$ of that of the $B2$ phase. However, the unit-cell volume of the $B19'$ phase is almost twice as large as that of the $B2$ phase, resulting in four atoms (two Ni atoms and two Ti atoms) in the unit cell for the $B19'$ phase. Therefore, we believe that the smaller number of tetrahedra for the $B19'$ phase will cause little error. Effects of the quasiparticle self-energy are included by the methods described elsewhere.[24]

IV. RESULTS AND DISCUSSION

The measured OC spectra are shown in Fig. 1. In the measured energy range the interband transitions are predominant. We can clearly see two structures in the spectrum of the $B2$ phase: one peak at ~2.26 eV and one shoulder at ~3.5 eV. At the MT the intensity of the lower peak increases. The magnitude of the upper shoulder decreases and the spectrum of the $B19'$ phase has an almost indiscernible

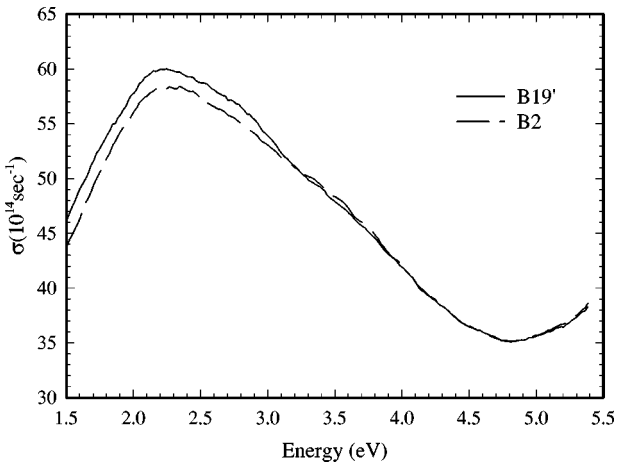

FIG. 1. The OC spectra of the $B2$ phase (solid line) and $B19'$ phase (dashed line) of the equiatomic NiTi alloy. Note that the zero of the optical conductivity is suppressed.

structure around 3.5 eV. On the other hand, a new structure appears at ~2.85 eV. Most of the interesting change in the OC at the MT occurs in the infrared (IR) region.[23] However, we could not measure the IR region because of the spectral limitation of our measurement system. General shapes of the spectra and the trend of change upon MT is very similar to the previous measurements.[23] However, there are some differences.

First, we could not observe peaks at 2.65 and 3.2 eV for the $B2$ phase and a peak at 2.65 eV for the $B19'$ phase, all of which were reported in Ref. 23. Rather, we observed a weak shoulder at ~3.5 eV for both phases and another weak shoulder ~2.85 eV in the $B19'$ phase. Although we observed a weak shoulder around 3.5 eV for the $B19'$ phase, it is so weak that it is almost indiscernible. Second, the magnitude of the OC measured by us is 35–50 % higher than that of Ref. 23 in the measured energy range.

In the previous measurements,[23] the 3.5-eV peak for the $B2$ phase gets weaker and becomes just a weak shoulder upon MT. The trend is consistent with our measurements. And the fact that the lower-energy peak increases upon MT is also consistent with our results. However, the region around 2.8 eV needs to be understood more clearly.

The difference in magnitudes of the OC between the previous measurements[23] and ours can be explained by the different methods of sample preparation. The authors of Ref. 23 electropolished the sample in an aged chloroacetic electrolyte (20% $HClO_4$ + 80% acetic anhydride by volume) after mechanical polishing. Electropolishing makes the sample surface rough, because of nonuniform removal of the surface layer, and leaves some chemical overlayer. The surface roughness decreases the measured OC.[25,30] The chemical overlayer may or may not decrease the OC. Although electropolishing may reduce the magnitude of the measured OC, it has one advantage. Since it removes the cold-work layer and reveals the crystal structure, the measured spectra may carry more accurate information on interband transitions. Our sample was only mechanically polished and, hence, the surface is almost ''amorphous'' and the sharp structure viewed in the spectra of Ref. 23, especially the 2.65-eV peak for both phases and the 3.2-eV peak for the $B2$ phase, may smear out. This kind of smearing in the measured dielectric functions for an amorphous material versus that of the corresponding crystalline one is seen in a-Si.[31]

However, in our sample the smearing of the 2.65-eV peak, due to the amorphization or deformation of the sample surface by mechanical polishing, is unlikely because we measured the OC spectrum of the $B19'$ phase after the UHV chamber and the sample were cooled down to room temperature after baking and, then, the sample holder was cooled down by the closed cycle helium refrigerator. As shown in Refs. 32 and 33, the baking of the UHV chamber at 150 °C can easily recrystallize the damaged surface due to mechanical polishing. In addition, the calculation (see below) shows no structure around 2.6 eV for the $B2$ phase. Therefore, we argue that there is no peak around 2.65 eV for the $B2$ phase; however, there must be some interband transition enhancement in the $B19'$ phase.

In order to understand these changes we carried out the band structure and OC spectra calculations. The band structures for the $B19'$ phase along some high-symmetry lines are

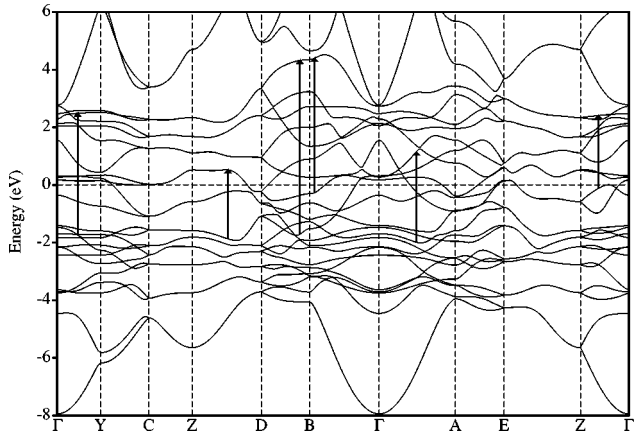

FIG. 2. Band structure of NiTi in the monoclinic ($B19'$) structure along some high-symmetry lines. The optical direct interband transitions corresponding to the measured peaks are denoted by the arrows.

shown in Fig. 2. (See Fig. 4 of Ref. 33 for the $B2$ phase.) The arrows drawn in the figures denote the direct interband transitions, which have prominent intensities. There are, of course, other transitions, which are still strong but not along the high-symmetry lines. This will be discussed later.

For the $B2$ phase the band structures are very similar to most other calculations.[11,13,16–18] However, there are some discrepancies. The lowest eight bands around the M point are located below the Fermi level in Ref. 18, while only the lowest six bands are below the Fermi level in Ref. 11 and Ref. 17. The bottom of the seventh band in the Γ-M direction slightly touches the Fermi level at 3/4 of the way to the M point in Ref. 11 and Ref. 17 but not in Ref. 18. Our calculation shows the same results as Ref. 11 and Ref. 17, except for our inclusion of spin-orbit splitting of some bands along some high-symmetry lines and points.

For the $B19'$ phase the calculated band structure shows a larger number of bands than that of the $B2$ phase, because of more atoms in the unit cell (two atoms per unit cell for the $B2$ phase and four atoms for the $B19'$ phase) and is very similar to that of Refs. 20 and 21 except for the spin-orbit splitting. One slight difference exists: the 16th band at the B point may or may not be occupied in Ref. 20, while our calculation, as well as that of Ref. 21, shows that it is unoccupied.

Our DOS curves for the both phases are essentially the same as those of Ref. 21, since we used the same crystal structure newly refined by Kudoh *et al.*[26] However, for the $B19'$ phase the DOS curves calculated by Ye, Chan, and Ho[21] and by us have a different shape from those calculated by Bihlmayer, Eibler, and Neckel,[20] who used the old crystal structure data.[1] The most striking result is that the Fermi level falls on a relatively deep local minimum of DOS curves in our calculations and in those of Ye, Chan, and Ho, while in Ref. 20 it is located at a rising edge of the DOS. The location of the Fermi level at a local minimum of the DOS is closely related to the stability of the crystal structure. As shown by Ye, Chan, and Ho[21] the $B19'$ phase has the lowest total energy among the competing structures, $B2$, $B11$, $B19$, and $L1_0$. Although the DOS of the $B2$ phase in Ref. 21 has a shallow local minimum at the Fermi level, ours does not have any local minimum in the vicinity of the Fermi level (see Fig. 5 of Ref. 33). Also, the greatest stability and the strongest covalency of FeTi among three transition-metal titanides (FeTi, CoTi, and NiTi) in the $B2$ phase was explained by the fact that only FeTi has a deep minimum in the DOS at the Fermi level, while it is located at a shallow local minimum (CoTi) or at a rising edge (NiTi) of DOS.[33] This has the consequence that the stability of the three alloys in the $B2$ phase is on the order (FeTi$>$CoTi $>$NiTi). Therefore, we conclude that the newly discovered crystal structure[26] for the $B19'$ phase NiTi is more suitable than the old one[1] and gives a better description of DOS and structural stability for the $B19'$ phase.

TABLE II. Fitting parameters for the real (λ) and imaginary (A and $E_{\max}$) parts of the self-energy.

	A (eV)	$E_{\max}$ (eV)	λ
$B2$	0.15	2.5	−0.20
$B19'$	0.12	2.5	−0.10

The calculated OC spectra were broadened by an energy-dependent Lorentzian function of width given by $\Gamma(E) = AE^2$ eV, where $E=[E_f(\mathbf{k})-E_i(\mathbf{k})]$, in eV, to simulate the effects of the imaginary part of the quasiparticle self-energy and the instrumental resolution. We set the limit for $\Gamma(E)_{\max}=2.5$ eV. After broadening the overall shape of the calculated spectra are similar to that of the measured ones, however, the energy positions of peaks and shoulders do not match. Therefore we used the real part of self-energy correction described in Ref. 24. The corrected optical conductivity, $\hat{\sigma}(\hat{\omega})$, is given by

$$\hat{\sigma}(\hat{\omega}) = \frac{1}{1+\lambda}\sigma\left(\frac{\omega}{1+\lambda}\right),$$

where $\sigma(\omega)$ is the uncorrected optical conductivity. The parameter λ has the effect of changing the excited-state energies $\hat{E}_n(\mathbf{k})$ relative to the energies, $E_n(\mathbf{k})$, calculated from the ground-state potential, given by

$$\hat{E}_n(\mathbf{k}) = E_n(\mathbf{k}) + \lambda[E_n(\mathbf{k}) - E_F]. \quad (1)$$

Although the parameter λ is dependent on the band index n and the wave vector $\mathbf{k}$, we assumed it to be constant. Therefore, the introduction of the parameter λ does not create any new features in the OC spectrum but just shifts the whole spectrum to lower or higher energy depending on the sign of λ. It also reduce or enhance the magnitude of the spectrum. The self-energy effects, due to the increase of energy of excited states below the Fermi level relative to the energy calculated from the ground-state potential, may lower the energy position of the calculated spectral features to the measured one.[34] It is not difficult to find the similar effects.[24,33–35] The fitting parameters, A, $\Gamma(E)_{\max}$, and λ, are summarized in Table II. As shown in Fig. 8 of Ref. 33 for the $B2$ phase and Fig. 3 for the $B19'$ phase, the broadening and self-energy correction markedly improve the agreement between experimental and theoretical OC spectra. For the purpose of comparison for both phases we redraw the theoretical spectra in Fig. 4. As can be seen in Fig. 4, all three changes observed in the experiments (enhancement of the

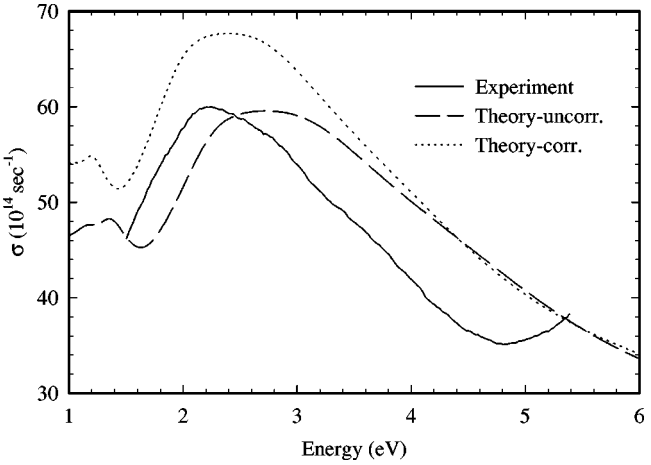

FIG. 3. Comparison of experimental and theoretical optical conductivity spectra for the $B19'$ phase. Two smoothed theoretical spectra (with and without self-energy correction) are shown. Note that the zero of the optical conductivity is suppressed.

2.26 peak, new structure at ~ 2.85 eV, and decrease of the 3.5-eV shoulder in the $B19'$ phase) are clearly evidenced in the theoretical calculations.

Previously, we made a comparative study of the OC spectra of FeTi, CoTi, and NiTi.[33] It was shown that the higher peak (~ 3.5 eV) is insensitive to the change of the number of valence electrons in a formula unit, while the lower peak (~ 2 eV) is very sensitive to the change. The band structure calculations show that the Fermi level moves ~ 1.0 eV to higher energy going from FeTi to NiTi. This shift is sufficient to change the occupation of several bands near the Fermi level, resulting in an alteration of the low-energy peak and even a splitting in the FeTi alloy.

Although the MT could not shift the Fermi level this much, it is enough to change the band structure near the Fermi level and the shape of the Fermi surface, and so on. Therefore, the lower the optical-transition energy, the greater the possibility of involving bands near the Fermi level, either initial or final states, and the more sensitive to the MT. Our measured and calculated spectra are consistent with this; the changes in the 2.26-eV peak and the 2.85-eV shoulder are more sensitive to the MT than the 3.5-eV shoulder.

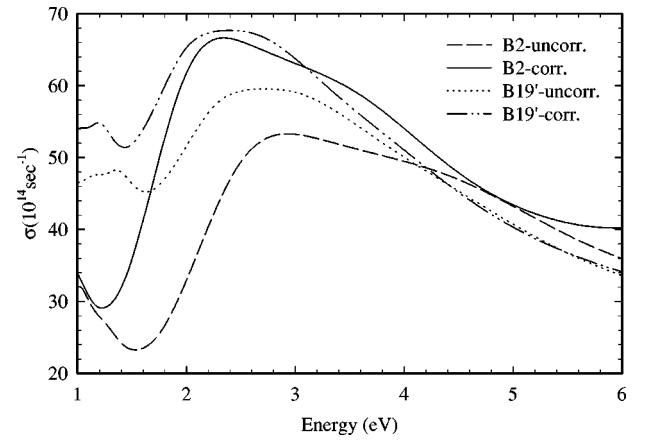

FIG. 4. Theoretical optical conductivity spectra for both phases. Spectra with and without self-energy correction are shown. Note that the zero of the optical conductivity is suppressed.

To understand the OC spectra and their change upon MT more thoroughly, it is desirable to know which parts of the BZ are predominantly involved in the optical transitions, especially those corresponding to the strong peaks and shoulders. For this purpose we analyzed the information on the **k** points and bands contributing strongly to the structures of the OC spectra. The **k** points whose optical transitions are strong along the high-symmetry lines are shown as arrows in Fig. 2 for the $B19'$ phase and Fig. 4 of Ref. 33 for the $B2$ phase.

For the $B2$ phase a large portion of the BZ near the Γ-X-M plane contributes to the 2.26 eV peak and the **k** points near the Γ-X-R plane also contribute. However, the latter is significantly weaker than the former. Other strong transitions were from some high-symmetry lines such as the Γ-X, Γ-M, and X-R lines, especially near the X point. The transitions involved in this peak are mainly 4th$\rightarrow$8th, 5th$\rightarrow$8th, and 6th$\rightarrow$9th. For the $B19'$ phase the **k** points contributing to the 2.26-eV peak are similar to those in the case of the $B2$ phase, if we convert the **k** vector into the coordinates of the $B2$ phase. The main transitions for the $B19'$ phase are 9th $\rightarrow$15th, 9th$\rightarrow$16th, 10th$\rightarrow$15th, 10th$\rightarrow$16th, and 14th $\rightarrow$20th, 21st, and 22nd. Although the characteristics of the **k** points and the band pairs for the 2.26-eV peak for both phases are similar to each other, there are very strong transitions for the $B19'$ phase from band 14 to bands 20, 21, and 22 that are absent in the $B2$ phase and these transitions are allowed because of the bands folded back from the $B2$ phase to the $B19'$ phase. The 14th band in these transitions is located near the Fermi level—approximately 0.02–0.26 eV lower than the Fermi level—and is sensitive to the MT. These newly allowed transitions give contributions to the increase of the OC in the $B19'$ phase.

For the 3.5-eV shoulder, the situation is very similar to the case of the 2.26-eV peak in the $B2$ phase. The only differences are the final states; they are in the 10th, 11th, and 12th bands. Although for the $B19'$ phase the portions of the BZ involved in this energy region are quite similar to those in the case of the $B2$ phase, the bands are somewhat different. There are still appreciable transitions from the 14th band to the 22nd, 23rd, and 24th bands and there are also significant contributions from the transitions fifth–seventh$\rightarrow$19th bands. However, in Ref. 19 it was shown that there is some but not a significant difference in JDOS between the $B2$ and $B19'$ phases and, hence, the strength of the transitions for the $B19'$ phase must be much weaker than that of the $B2$ phase due to the smaller transition matrix elements, resulting in the weakening of the 3.5-eV shoulder in the $B19'$ phase. We analyzed the band characters of the initial and final states of the transitions responsible for this peak. Bands 4, 5, and 7 (initial states) of the $B2$ phase have mainly Ni $3d$ character with very small Ti $4p$ character, and bands 11 and 12 (final states) have mainly Ti $3d$ character, but with an appreciable amount Ni $4p$, resulting in a significant magnitude of the transition matrix element. Bands 5, 6, and 7 (initial states) of the $B19'$ phase have mainly Ni $3d$ character and band 19 (final states) has mainly Ti $3d$ character. All the above bands have a negligible amount of p character, yielding a small magnitude of the transition-matrix element. The situation is quite similar to the case of the transitions from bands 10–15 to bands 22 and 23. The lower bands have either mainly Ni

$3d$ character (bands 10 and 15) or an admixture of Ni $3d$ and Ti $3d$ characters and the upper bands have mainly Ti $3d$ character (band 22) or an admixture of small amounts of all characters (Ni $4s,4p$, and $3d$ and Ti $4s,4p$, and $3d$) without any predominant character. Therefore, we argue that the weakening of the 3.5-eV shoulder in the $B19'$ phase is due to the reduction of the p character in the electronic wave function of the final states upon the MT.

Since a weak shoulder develops around 2.85 eV in the $B19'$ phase, we also investigated this region. The portion of the BZ for the $B2$ phase is similar to the case of the 2.26-eV peak, but, the initial states are lower bands than those of the 2.26-eV peak; bands 2, 3, and 4. Some other transitions, such as 5th$\rightarrow$10th and 6th$\rightarrow$10th, are also observed. For the $B19'$ phase these are transitions from bands 9–12 to bands 15–18. In this energy range the enhancement of the OC in the $B19'$ phase is also due to the newly allowed transitions between the folded-back bands.

Therefore, we can conclude that the change in the OC spectra in the measured energy range upon MT is due to the band folding-back for all three structures, change in the energy spectrum near the Fermi level for the emergence of 2.85-eV shoulder, and change in transition matrix elements for the 3.5-eV shoulder. The occupied bands (initial states) have mainly Ni d character with an admixture of Ti d character, and the unoccupied bands (final states) have predominantly Ti d character.

V. CONCLUSION

We measured the OC spectra for the $B2$ and $B19'$ phases of NiTi equiatomic alloy. Although we did not observe the rich features found in previous measurements,[23] we found some change upon MT. The electronic structure and the OC calculations were done for both phases. The agreement between experiments and calculations were fairly good after an energy-dependent Lorentzian broadening and the self-energy correction were included. The calculations show that the change of the OC spectra upon MT is due to transitions between the folded-back bands, the change in the energy spectrum near the Fermi level and the change in transition matrix elements. Since the MT alters the energy spectrum near the Fermi level, but not much for the levels far from the Fermi level, further study of the OC spectra in the IR region is needed for more accurate understanding of the effects on the optical properties upon MT.

ACKNOWLEDGMENTS

We wish to thank Dr. S. Shabalovskaya for providing us with an alloy sample and some helpful discussions. One of us (J.Y.R.) was supported by the Basic Science Research Institute Program, Ministry of Education, Project No. BRSI-97-2459. A part of the theoretical work was done by using a CRAY C-90 supercomputer in SERI, Korea. The Ames Laboratory is operated for the U.S. Department of Energy by Iowa State University under Contract No. W-7405-Eng-82.

[1] G. M. Michal and R. Sinclair, Acta Crystallogr., Sect. B: Struct. Crystallogr. Cryst. Chem. **37**, 1803 (1981).
[2] F. E. Wang, W. J. Buchler, and S. J. Pickart, J. Appl. Phys. **36**, 3232 (1965).
[3] F. E. Wang, B. F. DeSavage, W. J. Buchler, and W. R. Hosler, J. Appl. Phys. **39**, 2166 (1968).
[4] S. A. Shabalovskaya, A. I. Lotkov, I. I. Sasovskaya, A. G. Narmonev, and A. I. Zakharov, Solid State Commun. **32**, 735 (1979).
[5] G. V. Lashkarev, S. M. Solonin, A. V. Brodovoĭ, I. F. Martynova, M. V. Radchenko, A. L. Mirets, and N. V. Goncharuk, Fiz. Tverd. Tela (Leningrad) **34**, 658 (1992) [Sov. Phys. Solid State **34**, 352 (1992)].
[6] M. A. Mitchell, F. E. Wang, and J. R. Cullen, J. Appl. Phys. **45**, 3337 (1974).
[7] R. N. Lee and R. Withers, J. Appl. Phys. **49**, 5488 (1978).
[8] V. E. Egorushkin, Fiz. Tverd. Tela (Leningrad) **24**, 1276 (1982) [Sov. Phys. Solid State **24**, 725 (1982)].
[9] V. E. Egorushkin and S. E. Kulkova, J. Phys. F **12**, 2823 (1982).
[10] G. L. Zhao, T. C. Leung, B. N. Harmon, M. Keil, M. Müllner, and W. Weber, Phys. Rev. B **40**, 7999 (1989).
[11] G. L. Zhao and B. N. Harmon, Phys. Rev. B **48**, 2031 (1993).
[12] S. A. Shabalovskaya, Phys. Status Solidi B **132**, 328 (1985).
[13] D. A. Papaconstantopoulos, G. N. Kamm, and P. N. Poulopoulos, Solid State Commun. **41**, 93 (1982).
[14] M. B. Salamon, M. E. Meichle, C. M. Wayman, C. M. Whang, and S. M. Shapiro, in *Meson Nuclear Physics*, edited by E. V. Hungerford III, AIP Conf. Proc. No. **53**, 233 (AIP, New York, 1979); M. E. Meichle, Ph.D. thesis, University of Illinois, 1981; S. K. Sajita, S. M. Shapiro, and M. B. Salamon, Bull. Am. Phys. Soc. **26**, 381 (1981); M. E. Meichle, M. B. Salamon, and C. M. Wayman, *ibid.* **26**, 381 (1981).
[15] O. Mercier, K. N. Melton, G. Gremaud, and J. Hägi, J. Appl. Phys. **51**, 1833 (1980).
[16] R. Eibler, J. Redinger, and A. Neckel, J. Phys. F **17**, 1533 (1987).
[17] G. Bilhlmayer, R. Eibler, and A. Neckel, Ber. Bunsenges. Phys. Chem. **96**, 1626 (1992).
[18] V. B. Lapin, V. E. Egorushkin, S. A. Shabalovskaya, and O. P. Ivanova, Solid State Commun. **73**, 471 (1990).
[19] S. E. Kulkova, V. E. Egorushkin, and V. V. Kalchikhin, Solid State Commun. **77**, 667 (1991).
[20] G. Bilhlmayer, R. Eibler, and A. Neckel, J. Phys.: Condens. Matter **5**, 5083 (1993).
[21] Y. Y. Ye, C. T. Chan, and K. M. Ho, Phys. Rev. B **56**, 3678 (1997).
[22] X. Wang, Y. Y. Ye, C. T. Chan, K. M. Ho, and B. N. Harmon, Phys. Rev. B **58**, 2964 (1998).
[23] I. I. Sasovskaya, S. A. Shabalovskaya, and A. I. Lotkov, Zh. Éksp. Teor. Fiz. **77**, 2341 (1979) [Sov. Phys. JETP **50**, 1128 (1979)].
[24] J. Y. Rhee, B. N. Harmon, and D. W. Lynch, Phys. Rev. B **55**, 4124 (1997).
[25] J. Y. Rhee, Ph.D. thesis, Iowa State University, 1992.
[26] Y. Kudoh, M. Tokonami, S. Miyazaki, and X. Otsuka, Acta Metall. **33**, 2049 (1985).
[27] D. D. Koelling and B. N. Harmon, J. Phys. C **10**, 3170 (1977).
[28] L. Hedin and B. I. Lundqvist, J. Phys. C **4**, 2064 (1971).
[29] O. Jepsen and O. K. Andersen, Solid State Commun. **9**, 1763 (1971).
[30] D. E. Aspnes, E. Kinsbron, and D. D. Bacon, Phys. Rev. B **21**,

3290 (1980).
[31] D. E. Aspnes, A. A. Studna, and E. Kinsbron, Phys. Rev. B **27**, 985 (1984).
[32] J. Y. Rhee (unpublished).
[33] J. Y. Rhee, B. N. Harmon, and D. W. Lynch, Phys. Rev. B **54**, 17 385 (1996).
[34] J. F. Janak, A. R. Williams, and V. L. Moruzzi, Phys. Rev. B **11**, 1522 (1975).
[35] D. G. Laurent, J. Callaway, and C. S. Wang, Phys. Rev. B **20**, 1134 (1979).